

# Enhanced photogalvanic effect in graphene due to Rashba spin-orbit coupling

M. Inglot,<sup>1</sup> V. K. Dugaev,<sup>1,2</sup> E. Ya. Sherman,<sup>3,4</sup> and J. Barnaś<sup>5,6</sup>

<sup>1</sup>*Department of Physics, Rzeszów University of Technology, al. Powstańców Warszawy 6, 35-959 Rzeszów, Poland*

<sup>2</sup>*Departamento de Física and CeFEMA, Instituto Superior Técnico, Universidade de Lisboa, av. Rovisco Pais, 1049-001 Lisbon, Portugal*

<sup>3</sup>*Department of Physical Chemistry, Universidad del País Vasco UPV-EHU, 48080 Bilbao, Spain*

<sup>4</sup>*IKERBASQUE Basque Foundation for Science, Bilbao, Spain*

<sup>5</sup>*Faculty of Physics, Adam Mickiewicz University, ul. Umultowska 85, 61-614 Poznań, Poland*

<sup>6</sup>*The Nano-Bio-Medical Centre, Umultowska 85, 61-614 Poznań, Poland*

(Received 6 February 2015; revised manuscript received 5 May 2015; published 21 May 2015)

We analyze theoretically the optical generation of a spin-polarized charge current (photogalvanic effect) and spin polarization in graphene with Rashba spin-orbit coupling. An external magnetic field is applied in the graphene plane, which plays a crucial role in the mechanism of current generation. We predict a highly efficient resonant photogalvanic effect in a narrow frequency range that is determined by the magnetic field. A relatively less efficient photogalvanic effect appears in a broader frequency range, determined by the electron concentration and spin-orbit coupling strength.

DOI: [10.1103/PhysRevB.91.195428](https://doi.org/10.1103/PhysRevB.91.195428)

PACS number(s): 72.80.Vp, 72.25.Fe, 78.67.Wj, 81.05.ue

## I. INTRODUCTION

Two-dimensional (2D) electron systems with spin-orbit (SO) coupling are currently attracting a broad interest due to the coupled charge and spin dynamics, as revealed in a variety of spin-related transport phenomena [1–4]. Due to the SO coupling, the spin dynamics can be generated, among others, by a low-frequency electric field [5] and optically by interband electronic transitions [6–8]. Moreover, an external static magnetic field can enable the current generation by light absorption, leading to a magnetogyrotropic photogalvanic effect [9] in 2D semiconductor structures of appropriate symmetry.

Many of the spin-related phenomena, including also the ones mentioned above, can be observed in 2D graphene monolayers and other graphenelike materials such as silicene. The huge interest in graphene is related mainly to its natural two-dimensionality, its very unusual electronic structure, its excellent transport properties due to high electron mobility [10,11], and a variety of intriguing light-matter interaction effects in a wide range of frequencies (see, e.g., Ref. [12]), including unusual nonlinear phenomena [13,14]. Even though the intrinsic SO interaction in free-standing graphene is negligibly small, the Rashba SO coupling can be rather strong, e.g., for graphene deposited on certain heavy-element substrates [15–17], in hydrogenated layers [18], and in proximity of topological [19], antiferromagnetic [20], and ferromagnetic [21] insulators. Since the electronic band structure of graphene is significantly different from that of a simple 2D electron gas (2DEG), and the SO coupling creates a gap in the electronic spectrum, graphene can reveal qualitatively new effects which cannot be observed in 2DEG in conventional semiconductor heterostructures. Additionally, the SO-related phenomena in graphene are also important from the point of view of potential applications in all-graphene-based spintronics devices [22–24].

Here we predict an enhanced resonant photogalvanic effect in SO-coupled graphene. To do this, we consider the charge current generated in graphene by optical pumping in the infrared photon energy region, and we show that the optical

pumping can be used to generate not only the spin density [25], but also a spin-polarized net current. Breaking of the symmetry by an external magnetic field applied in the graphene plane plays an important role in the mechanism of current generation. We show that the efficiency of current generation per absorbed photon can be very high at certain conditions. Apart from this, we also show that one can create spin density without creating electric current, but not *vice versa*.

## II. MODEL

We consider the low-energy electronic spectrum of graphene in the vicinity of Dirac points [11]. Additionally, we include the Rashba SO coupling [26] and the Zeeman energy in a weak in-plane magnetic field  $\mathbf{B}$ . The corresponding Hamiltonian can then be written in the form

$$\hat{H} = \hbar v_0(\pm\tau_x k_x + \tau_y k_y) + \lambda(\pm\tau_x \sigma_y - \tau_y \sigma_x) + \frac{\Delta}{2}(\mathbf{b} \cdot \boldsymbol{\sigma}), \quad (1)$$

where  $v_0 \simeq 10^8$  cm/s is the electron velocity in graphene,  $\tau_x$  and  $\tau_y$  are the Pauli matrices defined in the sublattice space,  $\Delta \equiv gB$  is the maximum Zeeman splitting,  $\mathbf{b} \equiv \mathbf{B}/B$ , while the + and – signs refer to the  $K$  and  $K'$  Dirac points, respectively. Furthermore,  $g = g_L \mu_B$ , with  $g_L = 2$  being the Landé factor, and  $\lambda = \alpha/2$ , with  $\alpha$  denoting the Rashba coupling constant [27].

The electronic spectrum corresponding to Hamiltonian (1) consists of four energy bands in each valley,  $E_{n\mathbf{k}}$ , where  $n = 1 - 4$  is the band index. The corresponding spectrum for  $B = 0$  is shown in Fig. 1(a), and it is given by the formula  $E_{n,\mathbf{k}}(B = 0) = \mp\lambda \pm \sqrt{\lambda^2 + \hbar^2 v_0^2 k^2}$ . In turn, the expectation value of the spin at  $B = 0$  is oriented perpendicularly to the wave vector  $\mathbf{k}$  [27], similar to a semiconductor-based 2DEG with Rashba SO coupling. Contrary to the 2DEG, there are, however, no eigenstates of Hamiltonian (1) with a definite eigenvalue of any spin component. This appears to be due to the specific form of the SO coupling in graphene. The corresponding spin components at  $B = 0$  for the wave vector  $\mathbf{k} \equiv k(\cos\theta, \sin\theta)$

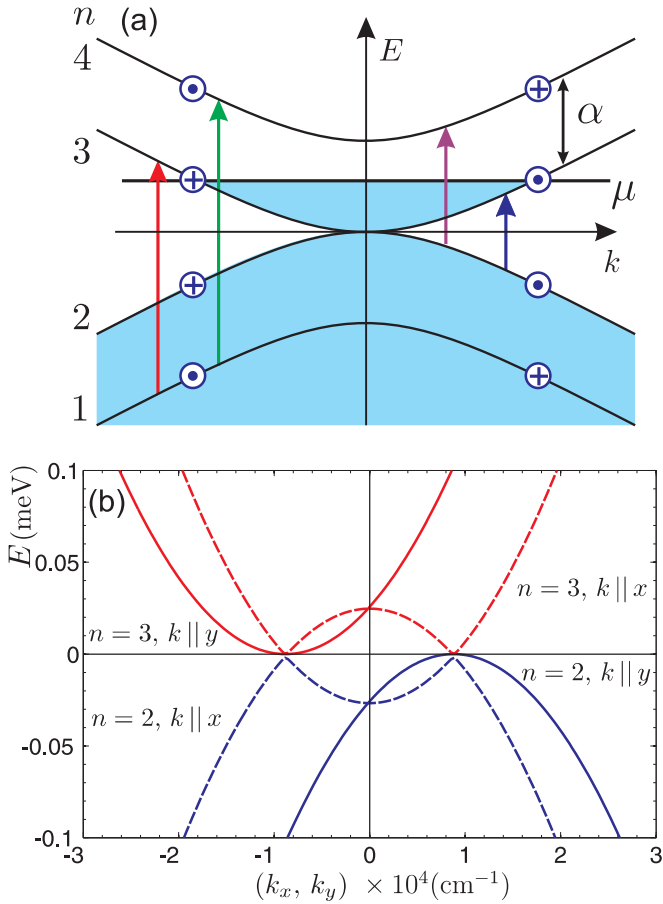


FIG. 1. (Color online) (a) Schematic picture of the band structure of graphene with Rashba SO interaction with all possible band transitions for a chosen chemical potential, indicated by the vertical arrows. Circles with crosses and dots inside correspond to the opposite spin orientations in the subbands. (b) Dispersion of the low-energy states for indicated wave-vector orientations. The band index is also marked at the plots. The assumed magnetic field  $\mathbf{B} \parallel x$  is equal to 5 T.

are

$$\langle \sigma_x(\mathbf{k}) \rangle_{B=0} = \mp \frac{v_k}{v_0} \sin \theta, \quad \langle \sigma_y(\mathbf{k}) \rangle_{B=0} = \pm \frac{v_k}{v_0} \cos \theta, \quad (2)$$

where  $v_k = v_0 \times \hbar v_0 k / \sqrt{\lambda^2 + \hbar^2 v_0^2 k^2}$  is the absolute value of the electron velocity at  $B = 0$ . Here the upper and lower signs correspond to the bands (1,4) and (2,3), respectively. Note that both spin components given by Eq. (2) vanish in the limit of  $k = 0$  [27] corresponding to the mixed rather than the pure character of the band states in the spin subspace.

The electronic spectrum presented in Fig. 1(a) is significantly modified by an external in-plane magnetic field. Assume this field is oriented along the axis  $x$ . The exact electronic spectrum obtained by direct diagonalization of the Hamiltonian (1) is shown in Fig. 1(b) for  $\mathbf{k} \parallel x$  and  $\mathbf{k} \parallel y$ . Only the states corresponding to the bands labeled in Fig. 1(a) with the index 2 and 3 are shown there. As one can note, for  $\mathbf{k} \parallel x$  the electron bands are shifted vertically, i.e., to higher (lower) energy, while for the other propagation direction the

bands are shifted horizontally, i.e., to the left (right) from the point  $k = 0$ . The latter separation in the  $\mathbf{k}$  space of bands 2 and 3 is crucial for the enhanced photogalvanic effect. For a weak Zeeman energy,  $\Delta \ll \alpha$ , and for the electron momenta of our interest,  $k \gg \sqrt{\alpha \Delta} / \hbar v_0$ , the field-dependent correction to the electron energy has the form

$$E_{n,k}(B) - E_{n,k}(B=0) = \mp \frac{\Delta}{2} \frac{v_k}{v_0} \sin \theta, \quad (3)$$

where again the upper and lower signs correspond to the bands (1,4) and (2,3), respectively.

Assume now that the system is subject to electromagnetic irradiation. The Hamiltonian describing the interaction of electrons in graphene with the external periodic electromagnetic field,  $\mathbf{A}(t) = \mathbf{A}_0 e^{-i\omega t}$ , takes the form

$$\hat{H}_A = \mp \frac{e}{c} v_0 (\boldsymbol{\tau} \cdot \mathbf{A}). \quad (4)$$

As in Eq. (1), different signs correspond here to electrons within the  $K$  and  $K'$  valleys.

The injection rate of a quantity  $O$ , related to the inter-subband optical transitions, can be calculated using Fermi's golden rule,

$$O(\omega) = \sum_{n,n'} O^{n \rightarrow n'}(\omega), \quad (5)$$

$$O^{n \rightarrow n'}(\omega) = \frac{2\pi}{\hbar} \int \frac{d^2 \mathbf{k}}{(2\pi)^2} |\langle \Psi_{n\mathbf{k}} | \hat{H}_A | \Psi_{n'\mathbf{k}} \rangle|^2 \hat{O}^{n \rightarrow n'} \times \delta(E_{n\mathbf{k}} + \hbar\omega - E_{n'\mathbf{k}}) f(E_{n\mathbf{k}}) [1 - f(E_{n'\mathbf{k}})],$$

where  $f(E_{n\mathbf{k}})$  is the Fermi-Dirac distribution function. Since there are two valleys,  $K$  and  $K'$ , one needs to calculate contributions to  $O(\omega)$  from both of them. The quantities of interest here are

$$\hat{O}^{n \rightarrow n'} \equiv \hat{\mathbb{1}} \quad (6)$$

for the light absorption (where  $\hat{\mathbb{1}}$  is the identity operator),

$$\hat{O}^{n \rightarrow n'} \equiv \langle \Psi_{n'\mathbf{k}} | \sigma_v | \Psi_{n\mathbf{k}} \rangle - \langle \Psi_{n\mathbf{k}} | \sigma_v | \Psi_{n'\mathbf{k}} \rangle \quad (7)$$

for the corresponding spin component injection, and

$$\hat{O}^{n \rightarrow n'} \equiv \langle \Psi_{n'\mathbf{k}} | \hat{I}_i | \Psi_{n\mathbf{k}} \rangle - \langle \Psi_{n\mathbf{k}} | \hat{I}_i | \Psi_{n'\mathbf{k}} \rangle \quad (8)$$

for the current generation. Here,  $\hat{I}_i \equiv e \hat{v}_i$ , where  $e$  is the electron charge, while  $\hat{v}_x \equiv \pm v_0 \tau_x$  and  $\hat{v}_y \equiv v_0 \tau_y$ .

### III. RESULTS

Using equations (5)–(8) for the injection rate, one can calculate the charge current and spin polarization induced by the optical pumping. Let us begin with the photogalvanic effect, i.e., charge current generation. Results for two different polarizations of the electromagnetic field  $\mathbf{A}(t)$  are presented in Figs. 2 and 3. Here the injection efficiency  $\tilde{I}_i$  is defined as  $\tilde{I}_i \equiv I_i / e v_0 \mathcal{I}_0$ , where  $\mathcal{I}_0 = \pi e^2 Q / \hbar c$  and  $Q$  is the incident photon flux [28–30].

The transitions start at  $\hbar\omega \approx 2\mu - \alpha$  if  $\mu \geq \alpha$  and at  $\hbar\omega \approx 2\mu$  otherwise. In both cases, a strong narrow peak in the injection efficiency appears at a resonant energy  $\hbar\omega \approx 2\mu$ . This peak is remarkably higher for the electromagnetic field polarized along the static magnetic field  $\mathbf{B}$ ; compare Figs. 2

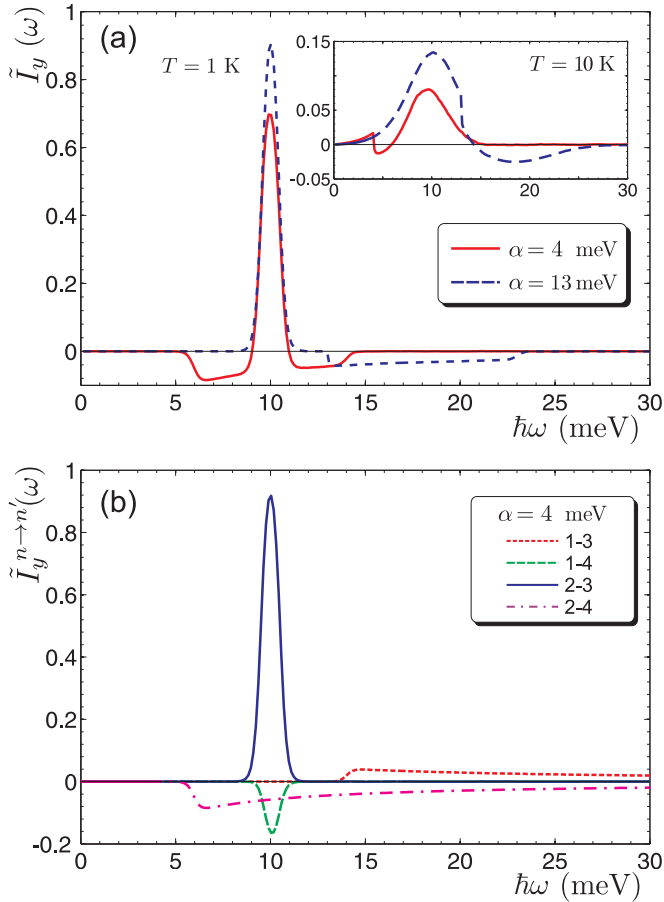


FIG. 2. (Color online) (a) Normalized charge current  $\tilde{I}_y$  in the case of low temperature,  $T = 1$  K ( $T = 10$  K in the inset). The Rashba SO coupling strength is  $\alpha = 4$  meV (solid red line) and  $\alpha = 13$  meV (dashed blue line). The chemical potential  $\mu = 5$  meV,  $\mathbf{B}$  is parallel to the  $x$  axis ( $B = 5$  T), while  $\mathbf{A} \parallel \mathbf{B}$ . (b) Contributions of indicated intersubband transitions to the total current presented in (a) for  $\alpha = 4$  meV.

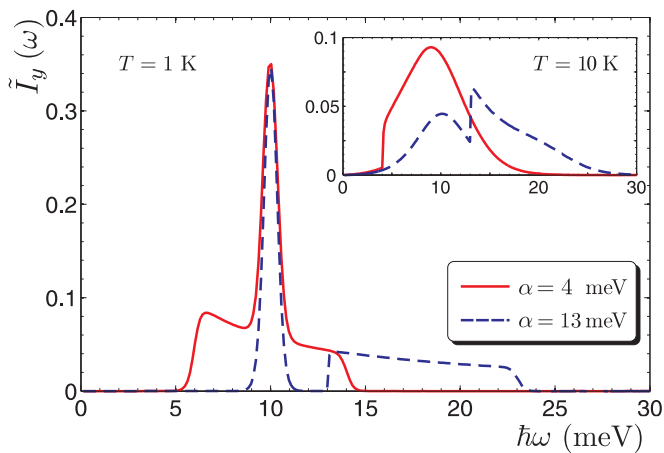


FIG. 3. (Color online) Normalized charge current  $\tilde{I}_y$  for low temperature,  $T = 1$  K ( $T = 10$  K in the inset). The solid red line is for  $\alpha = 4$  meV and the dashed blue line is for  $\alpha = 13$  meV. Chemical potential  $\mu = 5$  meV,  $\mathbf{B}$  is parallel to the  $x$  axis ( $B = 5$  T), and  $\mathbf{A} \perp \mathbf{B}$ .

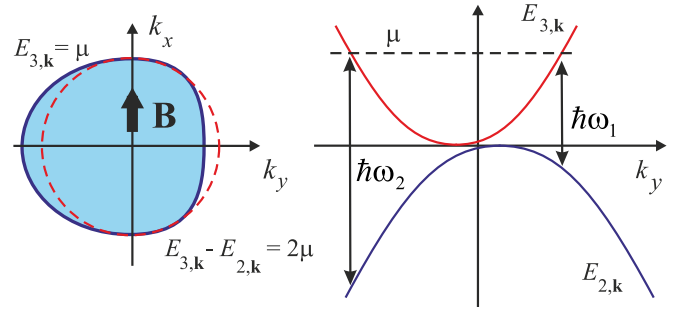


FIG. 4. (Color online) Left: Schematic picture of the Fermi line (solid) and resonance line (dashed) for the chosen subbands. Optical transitions are possible only at the part of the dashed line outside the filled area. Each transition generates a current of the order of  $2ev_{k_F}$ , making the generation highly efficient. Right: Side view of the intersubband transitions, which can occur in the frequency interval  $\omega_1 \leq \omega \leq \omega_2$ .

and 3. To understand the origin of this peak, let us consider transitions between the subbands marked with  $n = 2$  and 3. First, we determine the shape of the isoenergetic line corresponding to a given Fermi energy,  $\mu \gg \Delta$ . For the band corresponding to  $n = 3$ , one obtains from Eq. (3) the first-order correction to the Fermi wave vector,

$$\hbar k_F = \frac{\sqrt{\mu^2 + 2\lambda\mu}}{v_0} \mp \frac{\Delta}{2v_0} \sin \theta, \quad (9)$$

which sets the following boundaries for the Fermi surface:

$$-\frac{\sqrt{\mu^2 + 2\lambda\mu}}{v_0} - \frac{\Delta}{2v_0} < \hbar k_{F,y} < \frac{\sqrt{\mu^2 + 2\lambda\mu}}{v_0} - \frac{\Delta}{2v_0}, \quad (10a)$$

$$-\frac{\sqrt{\mu^2 + 2\lambda\mu}}{v_0} < \hbar k_{F,x} < \frac{\sqrt{\mu^2 + 2\lambda\mu}}{v_0}. \quad (10b)$$

Due to the  $\mathbf{k}$ -dependent Zeeman term, the Fermi surface becomes considerably deformed and anisotropic, as shown in the left panel of Fig. 4. The maximum deformation is independent of the chemical potential and SO coupling. In turn, the resonance line determined by  $E_{3,k} - E_{2,k} = \hbar\omega$  is still a circle given by the condition

$$\hbar k_\omega = \frac{\sqrt{\hbar^2 \omega^2 / 4 + \lambda \hbar \omega}}{v_0}. \quad (11)$$

A part of the resonance line is inside the occupied region (see Fig. 4, left panel). Therefore, we have an interval of photon energies,  $(\hbar\omega_1, \hbar\omega_2)$ , as shown in the right panel of Fig. 4, where the transitions occur for positive values of  $k_y$ , while the transitions with negative  $k_y$  (which would partially compensate for the current) are forbidden. As a result, a very efficient current injection occurs in this photon energy window, as visible in Fig. 2. In the considered regime of  $\mu \gg \Delta$ , this photon energy interval is determined by the conditions

$$\hbar\omega_1 = 2\mu - \Delta \frac{v_{k_F}}{v_0}, \quad \hbar\omega_2 = 2\mu + \Delta \frac{v_{k_F}}{v_0}, \quad (12)$$

which results in the peak width given by the formula

$$\hbar(\omega_2 - \omega_1) = 2 \frac{\sqrt{\mu^2 + 2\lambda\mu}}{\mu + \lambda} \Delta. \quad (13)$$

With the increase in temperature to  $T > \Delta$ , this effect becomes smeared out by thermal broadening of the Fermi distribution, and the injection rate decreases, as shown in the insets to Figs. 2 and 3.

Similar arguments can also be applied to the transitions between  $n = 1$  and 4 subbands. As a result, one gets a relatively small negative peak in the injection rate at  $\hbar\omega \approx 2\mu$ ; see Fig. 2(b). The weakness of this injection channel is due to a relatively small Fermi velocity in the subband 4 at  $\mu - \alpha \ll \alpha$ , while its reversed sign is due to the opposite spin orientation in these subbands, which results [similar to Eq. (10a) and Fig. 4] in a different shape of the Fermi surface, where the transitions begin to occur at  $k_y < 0$ . In the limit  $\alpha \ll \mu$ , the positive and negative contributions compensate each other, and the current injection efficiency tends to zero, as is expected in the absence of SO coupling.

Let us consider now briefly the broad structure in the injection rate. It is formed by the  $\mathbf{k}$  dependence of the transition matrix elements and velocity, and it has an efficiency of the order of  $\Delta/\alpha$ . The current injection stops at  $\hbar\omega \approx 2\mu + \alpha$ , where the contributions due to transitions between different bands compensate for each other. We also mention that for  $\mathbf{B} \parallel x$ , the charge current has only the  $y$  component for both polarizations of the incident light. When the graphene is illuminated with infrared radiation, with the spectral width larger than  $\alpha$  and  $\mu$ , contributions to the current from the narrow highly efficient resonant peak and from the broad relatively lowly efficient structure are of the same order of magnitude. To understand the maximum scale of the effect, we estimate the injected current density in the saturation strong intensity regime as  $e\rho(\mu)v_0\Delta$ , where  $\rho(\mu)$  is the density of states in band 3. This estimate yields a large value of  $\sim e \times 10^{16} \text{ s}^{-1} \text{ cm}^{-1}$ . The mechanism of current injection is independent of the disorder in the graphene layer, and the equilibrium current is determined by the balance of the independent injection and disorder-dependent relaxation rates. Although the actual injected current density is much lower than this estimate, it is sufficient for experimental observation.

For completeness, we address briefly the problem of spin and spin current injection [31]. For both incident light polarizations, one obtains a net spin polarization along the  $x$  and  $y$  axes. The numerical results are presented in Fig. 5(a) for the total spin polarization  $S_x$ , while Fig. 5(b) shows injected spin polarization associated with specific optical transitions. The physical mechanism of the optically injected spin polarization is rather clear: the spin-flip transitions are related to the above-mentioned fact that the eigenstates of Hamiltonian (1) are not the spin eigenstates, and breaking of the time-reversal symmetry in the magnetic field allows one to inject spin density. Since the charge current is along the  $y$  axis, we obtain effectively a spin-polarized current transferring in-plane spin components in the  $y$  direction.

#### IV. SUMMARY

We have calculated the optical injection of charge current in graphene as the photogalvanic effect due to SO coupling [32].

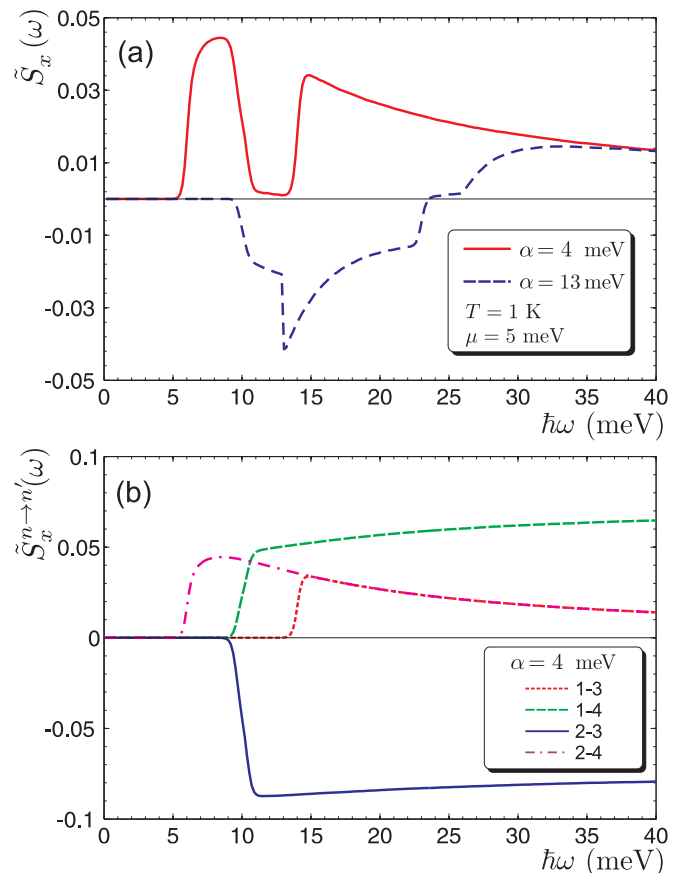


FIG. 5. (Color online) (a) Total injected normalized spin polarization  $\tilde{S}_x = \sum_{n,n'} \tilde{S}_x^{n \rightarrow n'}$ . Here the Rashba SO coupling  $\alpha = 4$  meV (solid red line) and  $\alpha = 13$  meV (dashed red line),  $\mu = 5$  meV, and  $B = 5$  T. The orientations of  $\mathbf{A}$  and  $\mathbf{B}$  are parallel to the  $x$  axis. (b) Transition-related spin injection  $\tilde{S}_x^{n \rightarrow n'}$ .

The current is injected only in a finite range of infrared light frequencies, determined by the chemical potential  $\mu$  and the SO coupling strength. The striking feature of this process is a narrow peak at the resonant frequency  $\hbar\omega \approx 2\mu$ , where the injection can be very efficient. Comparing the  $\omega$  dependence of the current and spin injection, we conclude that, depending on the light frequency, one can inject either spin-polarized electric current or spin polarization without the current injection. This result can be applied to a controllable current generation in SO-coupled graphene.

#### ACKNOWLEDGMENTS

This work is supported by the National Science Center in Poland under Grant No. DEC-2012/06/M/ST3/00042. The work of M.I. was supported by the project No. POIG.01.04.00-18-101/12. The work of E.Y.S. was supported by the University of Basque Country UPV/EHU under program UFI 11/55, Spanish Ministry of Economy and Competitiveness (FIS2012-36673-C03-01), and “Grupos Consolidados UPV/EHU del Gobierno Vasco” (IT-472-10).

- [1] *Spin Physics in Semiconductors*, edited by M. I. Dyakonov, *Springer Series in Solid-State Sciences* (Springer, Berlin, 2008).
- [2] J. Sinova, S. O. Valenzuela, J. Wunderlich, C. H. Back, and T. Jungwirth, [arXiv:1411.3249](https://arxiv.org/abs/1411.3249).
- [3] A. G. Aronov and Yu. B. Lyanda-Geller, *JETP Lett.* **50**, 431 (1989).
- [4] V. M. Edelstein, *Solid State Commun.* **73**, 233 (1990).
- [5] E. I. Rashba and A. L. Efros, *Phys. Rev. Lett.* **91**, 126405 (2003).
- [6] M. J. Stevens, A. L. Smirl, R. D. R. Bhat, A. Najmaie, J. E. Sipe, and H. M. van Driel, *Phys. Rev. Lett.* **90**, 136603 (2003).
- [7] Y. K. Kato, R. C. Myers, A. C. Gossard, and D. D. Awschalom, *Phys. Rev. Lett.* **93**, 176601 (2004).
- [8] A. Y. Silov, P. A. Blajnov, J. H. Wolter, R. Hey, K. H. Ploog, and N. S. Averkiev, *Appl. Phys. Lett.* **85**, 5929 (2004).
- [9] V. V. Bel'kov, S. D. Ganichev, E. L. Ivchenko, S. A. Tarasenko, W. Weber, S. Giglberger, M. Olteanu, H.-P. Tranitz, S. N. Danilov, P. Schneider, W. Wegscheider, D. Weiss, and W. Prettl, *J. Phys. Condens. Matter* **17**, 3405 (2005); V. V. Bel'kov and S. D. Ganichev, *Semicond. Sci. Technol.* **23**, 114003 (2008).
- [10] A. K. Geim and K. S. Novoselov, *Nat. Mater.* **6**, 183 (2007).
- [11] M. I. Katsnelson, *Graphene: Carbon in Two Dimensions* (Cambridge University Press, Cambridge, 2012).
- [12] P. Olbrich, C. Drexler, L. E. Golub, S. N. Danilov, V. A. Shalygin, R. Yakimova, S. Lara-Avila, S. Kubatkin, B. Redlich, R. Huber, and S. D. Ganichev, *Phys. Rev. B* **88**, 245425 (2013).
- [13] C. Drexler, S. A. Tarasenko, P. Olbrich, J. Karch, M. Hirmer, F. Müller, M. Gmitra, J. Fabian, R. Yakimova, S. Lara-Avila, S. Kubatkin, M. Wang, R. Vajtai, P. M. Ajayan, J. Kono, and S. D. Ganichev, *Nat. Nanotech.* **8**, 104 (2013).
- [14] M. M. Glazov and S. D. Ganichev, *Phys. Rep.* **535**, 101 (2014).
- [15] Y. S. Dedkov, M. Fonin, U. Rüdiger, and C. Laubschat, *Phys. Rev. Lett.* **100**, 107602 (2008).
- [16] A. Varykhalov, J. Sánchez-Barriga, A. M. Shikin, C. Biswas, E. Vescovo, A. Rybkin, D. Marchenko, and O. Rader, *Phys. Rev. Lett.* **101**, 157601 (2008).
- [17] M. Zarea and N. Sandler, *Phys. Rev. B* **79**, 165442 (2009).
- [18] J. Balakrishnan, G. K. W. Koon, M. Jaiswal, A. H. Castro Neto, and B. Özyilmaz, *Nat. Phys.* **9**, 284 (2013).
- [19] K. H. Jin and S. H. Jhi, *Phys. Rev. B* **87**, 075442 (2013).
- [20] Z. Qiao, W. Ren, H. Chen, L. Bellaiche, Z. Zhang, A. H. MacDonald, and Q. Niu, *Phys. Rev. Lett.* **112**, 116404 (2014).
- [21] Z. Wang, C. Tang, R. Sachs, Y. Barlas, and J. Shi, *Phys. Rev. Lett.* **114**, 016603 (2015).
- [22] B. Trauzettel, D. V. Bulaev, D. Loss, and G. Burkard, *Nat. Phys.* **3**, 192 (2007).
- [23] W. Han, R. K. Kawakami, M. Gmitra, and J. Fabian, *Nat. Nanotech.* **9**, 794 (2014).
- [24] P. Seneor, B. Dlubak, M.-B. Martin, A. Anane, H. Jaffres, and A. Fert, *MRS Bull.* **37**, 1245 (2012).
- [25] M. Inglot, V. K. Dugaev, E. Y. Sherman, and J. Barnaś, *Phys. Rev. B* **89**, 155411 (2014).
- [26] C. L. Kane and E. J. Mele, *Phys. Rev. Lett.* **95**, 226801 (2005).
- [27] E. I. Rashba, *Phys. Rev. B* **79**, 161409 (2009).
- [28] V. P. Gusynin and S. G. Sharapov, *Phys. Rev. B* **73**, 245411 (2006).
- [29] A. B. Kuzmenko, E. van Heumen, F. Carbone, and D. van der Marel, *Phys. Rev. Lett.* **100**, 117401 (2008).
- [30] P. Ingenhoven, J. Z. Bernád, U. Zülicke, and R. Egger, *Phys. Rev. B* **81**, 035421 (2010).
- [31] For pure spin currents, see J. Rioux, and G. Burkard, *Phys. Rev. B* **90**, 035210 (2014). These currents are symmetric with respect to the time reversal, and, therefore, a magnetic field there can only produce changes proportional to  $B^2$ .
- [32] The proposed mechanism is qualitatively different from the coherent control approach of D. Sun, C. Divin, J. Rioux, J. E. Sipe, C. Berger, W. A. de Heer, P. N. First, and T. B. Norris, *Nano Lett.* **10**, 1293 (2010).